Structural mechanical simulation to optimize the sensor arm geometry to be implemented on cranial remodeling orthosis

Cite as: AIP Conference Proceedings **2425**, 200004 (2022); https://doi.org/10.1063/5.0081312
Published Online: 06 April 2022

F. Veloso, D. Miranda, Pedro Morais, et al.

Structural Mechanical Simulation to Optimize the Sensor Arm Geometry to Be Implemented on Cranial Remodeling Orthosis

F. Veloso[1,b)], D. Miranda[1,a)], Pedro Morais[1,c)], Helena R. Torres[1,d)], Roberto Laranjeira[2,e)], Mario Ruediger[3,f)], F. Miranda[4,5,6,g)], António C.M. Pinho[7,h)], and J. L. Vilaça[1,i)]

[1]*2Ai – School of Technology, IPCA, Barcelos, Portugal*
[2] *CeNTI - Centre for Nanotechnology and Smart Materials, Vila Nova de Famalicão, Portugal*
[3]*Department for Neonatology and Pediatric Intensive Care, Children's Hospital, Medical Faculty of TU Dresden, Germany*
[4]*Instituto Politécnico de Viana do Castelo, Rua Escola Industrial e Comercial de Nun'Álvares, 4900-347 Viana do Castelo, Portugal*
[5]*Center for Research and Development in Mathematics and Applications (CIDMA), Department of Mathematics, University of Aveiro, 3810-193 Aveiro, Portugal*
[6]*PROMETHEUS, Instituto Politécnico de Viana do Castelo, Rua Escola Industrial e Comercial de Nun'Álvares, 4900-347 Viana do Castelo, Portugal*
[7]*Department of Mechanical Engineering, School of Engineering, University of Minho, Guimarães, Portugal*

[a)]Corresponding author: damiranda@ipca.pt
[b)]fveloso@ipca.pt
[c)]pmorais@ipca.pt
[d)]htorres@ipca.pt
[e)]rlaranjeira@centi.pt
[f)]mario.ruediger@uniklinikum-dresden.de
[g)]fmiranda@estg.ipvc.pt
[h)]acmpinho@dem.uminho.pt
[i)]jvilaca@ipca.pt

Abstract. For the treatment of moderate and severe cases of deformational plagiocephaly, an asymmetrical deformation of the skull, a cranial remodeling orthosis (CRO) is used. For the development of a new CRO concept, a pressure sensor grid is placed inside the orthosis that will allow the monitoring of excessive pressures and incorrect CRO positioning throughout the treatment. To implement the sensor grid in the CRO, high mobility of the sensor arms structure that joins the several sensors of this grid is required, however, it is intended that this procedure does not damage the printed copper tracks on the sensor structure. In this study, computer simulations were performed to optimize the sensor arm structure geometry, minimizing undesirable mechanical behavior in the sensor structure when subjected to tensile forces and displacements applied during its placement in the CRO. It was observed that the different sensor arm structures geometries have different effects on the mechanical behavior of the sensor structure when subjected to tensile forces and tensile displacement. The zigzag curve geometry presents the best performance based on high mobility without intense strain on the structure that could damage the printed copper tracks.

Keywords: cranial remodeling orthosis, deformational plagiocephaly, capacitive sensors, simulation, structural mechanics.

INTRODUCTION

Deformational plagiocephaly (DP) is a skull deformation that may occur in 46.6% of newborns and can be caused by intrauterine pressures, during birth or in the first months of life [1]. In moderate to severe cases it is treated with physiotherapy between the 4th and 9th months of life, and in some cases with the use of a special

International Conference of Numerical Analysis and Applied Mathematics ICNAAM 2020
AIP Conf. Proc. 2425, 200004-1–200004-6; https://doi.org/10.1063/5.0081312
Published by AIP Publishing. 978-0-7354-4182-8/$30.00

helmet designated as cranial remodeling orthosis (CRO) [2]. This skull deformation may hinder the natural psychomotor development of the infant and influence mental and motor skills in later life [3].

The CRO has been used in moderate to severe cases of DP since the early 70s and has seen some improvements, mainly in new materials and the digitalization of the process. The traditional CRO consists of an inner foam layer and a thin, rigid outer shell [4]. The treatment with existing CROs still presents some complications, such as excessive pressure, pressure sores, incorrect positioning of the orthosis, and difficulty in tracking the treatment performance [5].

To improve the sensitivity and quality of treatment data provided to the health professionals, we intend to develop a new CRO concept, where pressure sensors will be placed inside the orthosis. Thus, it will be possible to continuously monitor the treatment, checking for excessive pressures and incorrect CRO positioning, record effective treatment times, and other relevant clinical features.

METHODOLOGY

In this work, we aim to study the mechanical behavior of the pressure sensors during their assembly on the outer shell. These consist of copper tracks printed on a 200 μm Kapton layer. These sensors will be placed between the rigid outer layer and the foam lining of the CRO. In the center of each pressure sensor there is a positioning hole. These positioning holes will enable the alignment with existing temporary pins on the outer shell, and on the side of the pressure sensor facing the outer shell, there is an adhesive layer which affixes the sensors permanently after the positioning pins are removed from the outer layer.

A capacitive sensor grid is implemented on the outer surface of the CRO (Figure 1a)). This sensor grid is constituted by a set of sensor structures and each sensor is composed of two regions: sensor arms structure (SAS) and sensor pad structure (SPS) (Figure 1b)). The capacitive sensor will be positioned on the CRO through a pin inserted in hole A, as shown in figure 1b). In the successive implementation of several sensors, the SAS are required to be able to extend up to 2 mm. To extend the SAS, it will be necessary to apply tensile forces at SAS extremities of the fixed sensor. High mobility and low strain of the SAS are the optimization goals to prevent damage on the printed copper tracks.

In this context, a computer simulation was carried out to optimize the SAS geometry, with the objective of minimizing undesirable mechanical behavior in sensor structure when subjected to tensile forces applied during its placement in the CRO. According to this objective, it is important to implement theoretical simulations to optimize the SAS geometry to improve their mobility with low deformation (strain) of the sensor structure during the implementation of these sensors on the CRO. The theoretical simulations were performed by the Finite Element Method, applying the structural mechanics model. In the simulations developed, the pressure, strain, and displacement values were measured at different regions of the sensor structure (SAS and SPS) when tensile forces and tensile displacements were applied to SAS extremities (Figure 1b)). Three simulation tests were performed to study the mechanical behavior of one sensor structure with the different SAS geometries proposed. In tests 1 and 2, tensile forces (F1 and F2) with a magnitude of 90 N were applied to SAS extremities to evaluate the pressure, strain, and displacement caused on different structure sensor regions (SAS and SPS). Finally, in the third test, a displacement of 2 mm was applied to SAS extremities and the resulting strain was measured.

Figure 1b) shows the SAS geometries (linear geometry - A1, zigzag curve geometry - A2 and zigzag line geometry - A3), boundary conditions, measurement places (points and section line), and sensor structure dimensions that were applied in the simulation tests.

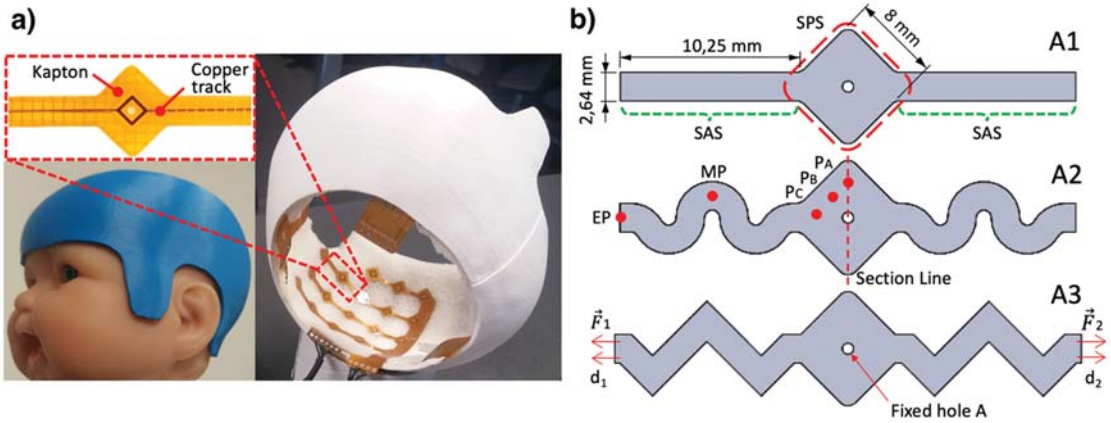

FIGURE 1. Schematic representation: **a)** capacitive sensor grid placed on the CRO and sensor structure detail (arms and pad), **b)** Sensor arms structure geometries (linear geometry - A1, zigzag curve geometry - A2 and zigzag line geometry - A3), boundary conditions, measurement places (Extreme Point – EP, Middle Point – MP, points – PA, PB, PC and section line) and sensor structure dimensions that applied in the simulations tests.

RESULTS AND DISCUSSION

The mechanical simulation tests were carried out on the sensor structure with different SAS geometries (A1, A2, and A3) to evaluate the pressure, strain, and displacement results at different sensor structure regions. In the first test, two tensile forces (F1 and F2) with a magnitude of 90 N were applied to SAS extremities with different geometries (figure 1b)). This is the minimum force required to stretch the SAS 1mm in the case of least mobility(A1). Figures 2a) and 2b) show the pressure and strain values measured on the section line at SPS (figure 1b)). According to figures 2a) and 2b), for different SAS geometries (A1, A2, and A3) the identical pressure and strain results were obtained along the section line of SPS.

For different SAS geometries, figures 2a) and 2b) show high pressure and strain values in the regions close to hole A of SPS (i.e. the location where the sensor structure is fixated to the CRO), respectively. Please note that on the margins of the SPS with hole A, the fixed constraint was established as a boundary condition at the simulation test (Figure 1b). Regarding A1, A2, and A3 geometrical configurations, figure 2c) shows the strain values obtained in three different points (PA, PB, and PC) that are located in a region where the copper tracks cross the SPS region. Figure 2c) shows that sensor structures A1, A2, and A3 have the same strain values at PA, PB, and PC points, with values of 1.3%, 2.4%, and 4.0%, respectively. It is important to note that the SAS geometrical configuration does not affect the mechanical behavior in the SPS region.

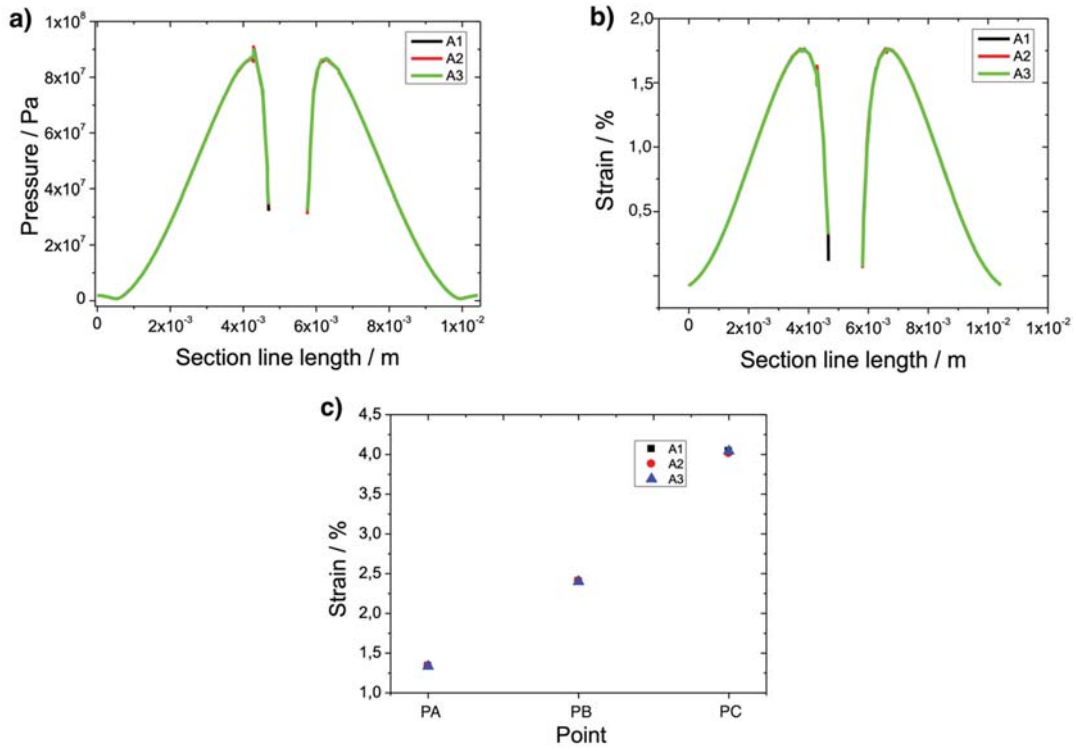

FIGURE 2. a) Pressure as a function of section line positions, **b)** Strain as a function of section line positions, **c)** Strain as a function of position points at sensor pad (PA, PB, and PC).

In the second test, the tensile forces F1 and F2 with a magnitude of 90 N were applied at SAS extremities of three geometries (A1, A2, and A3) to evaluate the displacement and strain values reached at two different SAS places characterized by a middle point (MP) and an extreme point (EP) (Figure 1b)).

At the middle point (Figure 3a)), for A1, A2, and A3 geometries the displacement values of 0.5 mm, 1.2 mm, and 1.0 mm were obtained, respectively. Consequently, the strain values of A1, A2, and A3 geometries obtained at MP point were 6.8%, 5.1%, and 6.1%, respectively.

Regarding the extreme point, Figure 3b) shows the displacement values of 1.2 mm, 5.7 mm, and 4.7 mm and strain values of 6.8%, 6.1%, and 6.8% at A1, A2, and A3 geometries, respectively. In both cases (MP and EP points), the A2 geometry presents a high SAS mobility. In contrast, the lowest mobility is attributed to A1 geometry.

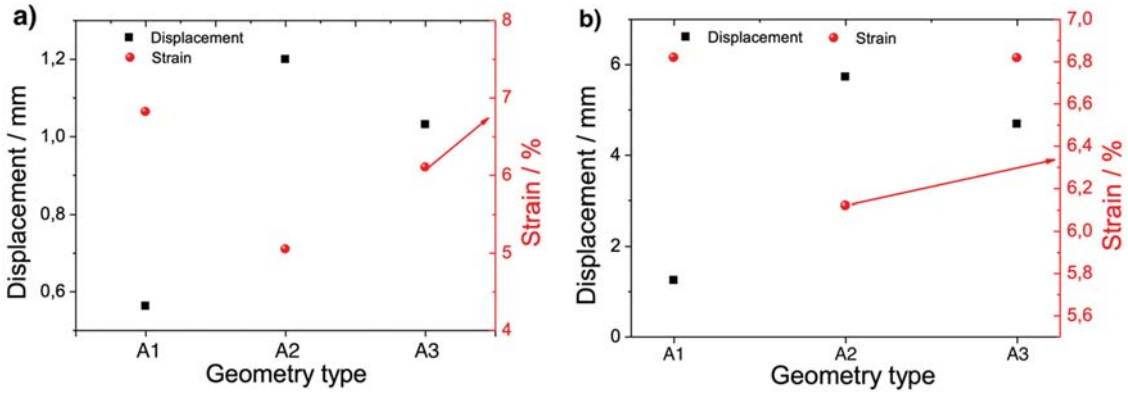

FIGURE 3. a) Displacement (black points) and strain (red points) as a function of SAS geometry type at middle point (MP), **b)** Displacement (black points) and strain (red points) as a function of SAS geometry type at extreme point (EP).

At the middle point, the A2 geometry shows a displacement increase of 140% and 20% related to A1 and A3 geometries, respectively. In the A2 geometry occurs a strain decrease of 25% and 16% compared to A1 and A3

geometries, respectively. In the cases of higher strain values such as A1 and A3, tensile forces may deform the sensor structure and damage the copper tracks printed on the Kapton structure (Figure 1a)).

At the extreme point, this effect is intensified because the mobility is further facilitated in more distant locations of the fixed sensor pad. The A2 geometry shows a displacement increase of 375% compared to A1 geometry and maintains a low strain value (Figure 3b)).

The mechanical behavior between A2 and A3 geometries is very similar. However, the A2 geometry shows slightly better performance based on high mobility and low strain of SAS. The A2 geometry shows a displacement increase of 21% and a strain decrease of 10% comparing to A3 geometry.

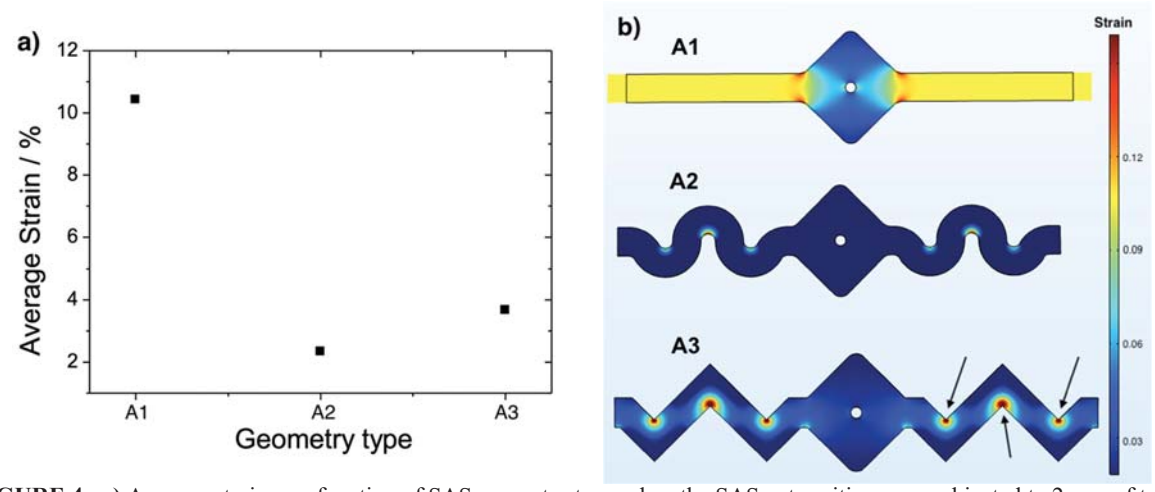

FIGURE 4. a) Average strain as a function of SAS geometry type when the SAS extremities were subjected to 2 mm of tensile displacement, **b)** 3D schematic representation of the strain gradient of the SAS geometry type when the SAS extremities were subjected to 2 mm of tensile displacement.

As previously mentioned, to implement the sensor capacitive grid in the CRO it is necessary to have a SAS mobility that allows a tensile displacement of its extremities up to 2 mm. Thus, in the last simulation test (third test), the average strain at SAS was measured when the SAS extremities were subjected to 2 mm of tensile displacement (d1 and d2), as shown in figure 1b). Figure 4a) shows the average strain values of 10.4%, 2.3%, and 3.7% at A1, A2, and A3 geometries, respectively. For the same tensile displacement of 2 mm, the A1 geometry has low mechanical stability, since it has a strain increase of 352% and 181% compared with A2 and A3 geometries, respectively. Both zigzag geometries (A2 and A3) show a structural configuration that allows high tensile mobility and the Kapton material of the SAS is subjected to low strain values, which minimizes possible damage to the copper tracks printed. Figure 4b) shows the strain gradients across the SAS. According to figure 4b), the A2 and A3 geometries have the lowest strain values (blue color), however, the A3 geometry presents critical zones with high strain values (red color). These critical zones are characterized by vertices of zigzag line structure (these zones are indicated by arrows in figure 4b)). The zigzag curve structure does not have these critical zones that increase the structure rupture probability.

CONCLUSION

In this work, the mechanical behavior of different 3D sensor arm structures geometries was theoretically evaluated when the sensor structure was subject to tensile forces and tensile displacements. To evaluate the different SAS geometries' performance, the pressures, strain, and displacements values were measured at different sensor structure regions. To improve the sensor arm structure performance, it is necessary to have a geometry that allows high mobility and low strain that prevents damage on the printed copper tracks. The sensor arm structure geometry with the best performance is the zigzag curve (A2). Both zigzag geometries (A2 and A3) show better mechanical performance compared to linear geometry (A1), however, the A2 geometry reaches a higher mobility degree with the lowest strain values. Moreover, the A2 structure has higher mechanical stability compared to the A3 geometry

once that the A3 geometry presents critical zones (vertices of the zigzag) with a high probability of rupture. Finally, it was observed that the different SAS geometries do not affect the mechanical behavior of the SPS region.

ACKNOWLEDGMENTS

This project was funded by Portuguese national funds (PIDDAC), through the FCT – Fundação para a Ciência e a Tecnologia and FCT/MCTES under the scope of the project UIDB/05549/2020. F. Veloso acknowledges "Fundação para a Ciência e a Tecnologia" (FCT), in Portugal, and the European Social Fund, European Union, for funding support through the "Programa Operacional Capital Humano" (POCH) in the scope of the Ph.D. grant SFRH/BD/131545/2017. This work has been supported by "SmartORTHOSIS - Ortótese inteligente personalizada para plagiocefalia posicional", with the reference NORTE-01-0145-FEDER- 024300, financed by the "Fundo Europeu de Desenvolvimento Regional (FEDER)", by "Programa Operacional Regional do Norte" (NORTE2020), and by Fundação para a Ciência e a Tecnologia (FCT). F. Miranda was supported by the Portuguese Foundation for Science and Technology (FCT – Fundação para a Ciência e a Tecnologia), through CIDMA – Center for Research and Development in Mathematics and Applications, within project UIDB/04106/2020. D. Miranda was also funded by the project "NORTE-01-0145-FEDER-000045", supported by Northern Portugal Regional Operational Programme (Norte2020), under the Portugal 2020 Partnership Agreement, through the European Regional Development Fund (FEDER).

REFERENCES

1. M. M. Boere-Boonekamp and L. T. van der Linden-Kuiper LT, "Positional preference: prevalence in infants and follow-up after two years," *Pediatrics*, vol. 107, no. 2, pp. 339–43, Feb. 2001.
2. A. B. K. Flannery *et al.*, "Evidence-Based Care of the Child With Deformational Plagiocephaly, Part II: Management," *J. Pediatr. Heal. Care*, vol. 26, no. 5, pp. 320–331, Sep. 2012, doi: 10.1016/j.pedhc.2011.10.002.
3. M. Fabre-Grenet, P. Garcia-Méric, V. Bernard-Niel, V. Guagliardo, S. Cortaredona, and M. Aymeric-Ponsonnet, "Effects of deformational plagiocephaly during the first 12 months on the psychomotor development of prematurely born infants," *Arch. Pediatr.*, vol. 24, no. 9, 2017, doi: 10.1016/j.arcped.2017.01.022.
4. T. R. Littlefield, "Cranial remodeling devices: Treatment of deformational plagiocephaly and postsurgical applications," *Semin. Pediatr. Neurol.*, vol. 11, no. 4, pp. 268–277, 2004, doi: 10.1016/j.spen.2004.10.004.
5. W. C. Gump, I. S. Mutchnick, and T. M. Moriarty, "Complications associated with molding helmet therapy for positional plagiocephaly: a review," *Neurosurg. Focus*, vol. 35, no. 4, p. E3, Oct. 2013, doi: 10.3171/2013.5.FOCUS13224.